Photocatalytic Hydrogen Evolution on $ZnS-CuInS_2-AgInS_2$ Solid Solution Photocatalysts with Wide Visible Light Absorption Bands

Issei Tsuji,[†] Hideki Kato,[†] and Akihiko Kudo*[,†,‡]

Department of Applied Chemistry, Faculty of Science, Tokyo University of Science, 1-3 Kagurazaka, Shinjuku-ku, Tokyo 162-8601, Japan, and Core Research for Evolutional Science and Technology, Japan Science and Technology Agency (CREST, JST), Japan

Received December 7, 2005. Revised Manuscript Received January 30, 2006

Pt-loaded $ZnS-CuInS_2-AgInS_2$ solid solutions showed photocatalytic activities for H_2 evolution from aqueous solutions containing SO_3^{2-} and S^{2-} as sacrificial reagents under visible light irradiation ($\lambda \geq 420$ nm). The crystal structures of the solid solutions were either zinc blende or wurtzite, depending on the composition. The diffuse reflectance and photoluminescence spectra of the solid solutions were shifted monotonically to longer wavelengths as the ratio of $MInS_2$ (M = Cu and Ag) to ZnS increased, indicating that the energy band structure of the sold solution was controllable by the change in the composition. The $ZnS-CuInS_2-AgInS_2$ solid solutions exhibited absorption bands that were longer in wavelength than those for the $ZnS-CuInS_2$ and $ZnS-AgInS_2$ solid solutions, which is probably due to interactions between the Cu 3d and Ag 4d orbitals. The photocatalytic activity for H_2 evolution was much improved by low-temperature synthesis (773−873 K) and the loading of Ru cocatalysts. The Ru-loaded $Cu_{0.25}Ag_{0.25}In_{0.5}ZnS_2$ solid solution, which had a wide absorption band (band gap, 1.77 eV) in the visible light region, showed high activity for H_2 production, even under simulated solar irradiation (AM 1.5).

1. Introduction

Photocatalytic reactions occurring under solar illumination have attracted attention for the development of fossil-fuel-independent energy systems for hydrogen production. Taking the solar spectrum into account, it is indispensable to develop a visible-light-driven photocatalyst. Sulfides, which have narrow band gaps (BGs) and valence bands at relatively negative potentials compared to oxides, can be good candidates for visible-light-driven photocatalysts. Sulfide photocatalysts such as CdS are not suitable for water splitting, because photocorrosion is induced when photogenerated holes oxidize the photocatalyst itself.[1] However, the presence of sacrificial hole scavengers such as sulfide and sulfite ions suppresses the photocorrosion and improves the photocatalytic activity for H_2 evolution under visible light irradiation. Photocatalytic reactions that make use of sacrificial reagents do not constitute complete water-splitting reactions but instead are water-splitting half reactions, which are often used as test reactions to establish whether materials are capable of reducing H_2O to form H_2. If byproducts such as hydrogen sulfide, which is emitted during the desulfurization process at chemical plants, can be turned into useful sacrificial reagents, such sacrificial photocatalytic reactions for hydrogen production will become extremely interesting from the viewpoint of energy and environmental issues. These concepts have been reported for a hydrogen production system aimed at byproduct utilization with a CdS photocatalyst.[2,3]

Most of the highly active photocatalysts for water splitting are wide band gap semiconductors, which respond only to ultraviolet light. In particular, tantalates and niobates, for example, $NaTaO_3$:La and $Sr_2Nb_2O_7$, have exhibited extremely high apparent quantum yields.[4−6] "Band engineering" is one of the strategies for the development of visible-light-driven photocatalysts for wide band gap photocatalysts.[7] The doping of foreign elements into wide band gap photocatalysts is often carried out. The authors have previously succeeded in the development of visible-light-driven photocatalysts by the doping of metal cations such as Ni^{2+},[8] Cu^{2+},[9] and Pb^{2+} [10] into ZnS, which is a highly active sulfide photocatalyst for hydrogen evolution, even without a Pt cocatalyst, under ultraviolet light irradiation.[11] Making a solid solution between wide and narrow band gap semiconductors is also a powerful strategy for band gap control. We have focused attention on the wide band gap photocatalyst ZnS and narrow band gap semiconductors, such as $AgInS_2$ and $CuInS_2$, that are similar to ZnS in crystal structure. The solid solutions showed higher activities than metal-ion-doped ZnS photocatalysts.[12,13]

* Author to whom correspondence should be addressed. Phone: +81-3-5228-8267. Fax: +81-3-3235-2214. E-mail: a-kudo@rs.kagu.tus.ac.jp.
[†] Tokyo University of Science.
[‡] Japan Science and Technology Agency.

(1) Pleskov, Y. V.; Gruevich, Y. Y. *Semiconductor Photoelectrochemistry*; Bartlett, P. N., Ed.; Plenum: New York, 1986.
(2) Linkous, C. A.; Mingo, T. E.; Muradov, N. Z. *Int. J. Hydrogen Energy* **1993**, *19*, 203.
(3) March, S. C.; Borrell, L.; Gimenez, J.; Simarro, R.; Andujar, J. M. *Int. J. Hydrogen Energy* **1992**, *17*, 683.
(4) Kato, H.; Asakura, K.; Kudo, A. *J. Am. Chem. Soc.* **2003**, *125*, 3082.
(5) Kato, H.; Kudo, A. *Catal. Today* **2003**, *78*, 561.
(6) Hwang, D. W.; Kim, H. G.; Kim, J.; Cha, K. Y.; Kim, Y. G.; Lee, J. S. *J. Catal.* **2000**, *193*, 40.
(7) Kudo, A.; Kato, H.; Tsuji, I. *Chem. Lett.* **2004**, *33*, 1534.
(8) Kudo, A.; Sekizawa, M. *Chem. Commun.* **2000**, 1371.
(9) Kudo, A.; Sekizawa, M. *Catal. Lett.* **1999**, *58*, 241.
(10) Tsuji, I.; Kudo, A. *J. Photochem. Photobiol., A* **2003**, *156*, 249.
(11) Reber, J. F.; Meier, K. *J. Phys. Chem.* **1984**, *88*, 5903.
(12) Tsuji, I.; Kato, H.; Kobayashi, H.; Kudo, A. *J. Am. Chem. Soc.* **2004**, *126*, 13406.

10.1021/cm0527017 CCC: $33.50
Published on Web 03/01/2006

The solid-solution-type photocatalysts have several advantages compared to the doped photocatalysts. First, the potentials of the conduction and valence bands shift successively with composition. Moreover, the solid solution photocatalyst is able to absorb enough visible light via the band gap transition, which is different from the doped photocatalyst, in which the electronic transition is from donor levels originating from dopant metal ions to the conduction band of the host material. Second, photogenerated electrons and holes are able to move smoothly in the continuous valence and conduction bands, but not in the discrete donor levels seen in the doped photocatalysts. As a solid solution sulfide photocatalyst, the CdS−ZnS system, which showed high photocatalytic activity for H_2 evolution, has been reported by Reber and Rusek and Kakuta et al.[14,15] Recently, Domen et al. have succeeded in overall water splitting on a GaN:ZnO solid solution under visible light irradiation ($\lambda > 400$ nm).[16,17]

In our previous communication, we preliminarily reported that the Ru-cocatalyst-loaded $ZnS-CuInS_2-AgInS_2$ solid solution showed high activity for hydrogen evolution, even under simulated solar irradiation.[18] In the present work, we prepared a series of $ZnS-CuInS_2-AgInS_2$ solid solutions [$= (CuAg)_xIn_{2x}Zn_{2(1-2x)}S_2$] to optimize the photocatalyst and systematically studied the relationship among the crystal structures, photophysical properties, and photocatalytic activities.

2. Experiment Section

Preparation and Characterization of Photocatalysts. An aqueous solution of $Zn(NO_3)_2 \cdot 6H_2O$ (Wako Pure Chemicals; 99.0%), $AgNO_3$ (Tanaka Kikinzoku; 99.8%), and $In(NO_3)_3 \cdot 3.6H_2O$ (Kojundo Chemical; 99.99%) with 10% excess amounts was purged with N_2 gas. CuCl was freshly prepared by the reduction of $CuCl_2 \cdot 2H_2O$ (Wako Pure Chemicals; 99.0%) with metallic Cu in boiling dilute hydrochloric acid and was then added into the solution. A grayish Cu−Ag−In−Zn sulfide precursor was precipitated by bubbling with H_2S gas into the mixed solution. The precipitate was stirred for about 15 h, washed with pure water, and dried in the air. The powder obtained was sealed in a quartz ampule in vacuo and heat treated at 673−1123 K in a tube furnace to synthesize the solid solution photocatalysts. The products were confirmed by X-ray diffraction (XRD; Rigaku MiniFlex). Surface areas were determined by the N_2 Brunauer−Emmett−Teller (BET) method (Coulter SA3100). Diffuse reflectance spectra were obtained with a UV−visible/near-IR spectrometer (Jasco Ubest U-570) and were converted from reflectance to absorbance by the Kubelka−Munk method. Photoluminescence spectra were measured in vacuo at 80 K with a spectrofluorometer (Spex FluoroMax). X-ray photoelectron spectra were measured with an X-ray photoelectron spectrometer (VG Scientific ESCALAB-MKU). Binding energies were corrected by use of the Zn 3d peak of ZnS at 10.5 eV.[19] Photocatalyst powders were observed by scanning electron microscopy (SEM; JEOL JSM-7400F and Hitachi S-5000).

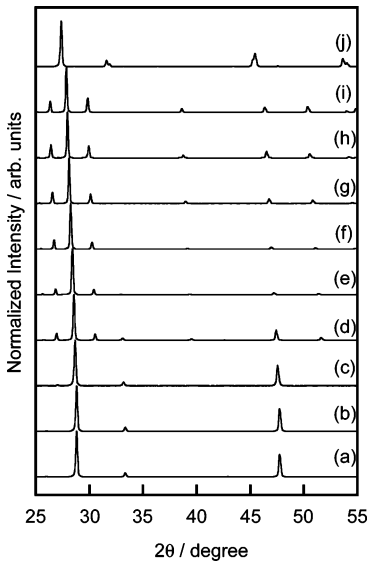

Figure 1. X-ray diffraction patterns of $(CuAg)_xIn_{2x}Zn_{2(1-2x)}S_2$ solid solutions; the values of x were (a) 0, (b) 0.01, (c) 0.025, (d) 0.05, (e) 0.1, (f) 0.15, (g) 0.20, (h) 0.25, (i) 0.30, and (j) 0.5. The samples were synthesized in a quartz ampule tube at 1123 K.

Photocatalytic Reactions. Photocatalytic reactions were conducted in a gas-closed circulation system. The photocatalyst powder (0.3 g) was dispersed by a magnetic stirrer in an aqueous solution (150 mL) containing K_2SO_3 and Na_2S as electron donors in a Pyrex cell with a top window. The photocatalysts were irradiated with visible light ($\lambda \geq 420$ nm) through a cutoff filter (Hoya L42) from a 300-W Xe lamp (ILC Technology; Cermax LX-300). The amount of H_2 evolved was determined with on-line gas chromatography (Shimadzu GC-8A, MS-5A column, TCD, Ar carrier). A solar simulator (Yamashita Denso YSS-80QA, AM 1.5) was also used. In this case, the amount of H_2 evolved was determined by a volumetric measurement. The photocatalytic powder was dispersed in a reactant solution containing an appropriate amount of $(NH_4)_2[RuCl_6]$ (Wako Chemicals; 29.9% as Ru) or $RhCl_3 \cdot nH_2O$ (Tanaka Kikinzoku) or $IrCl_3 \cdot nH_2O$ (Soekawa Rikagaku; 53% as Ir) or $H_2PtCl_6 \cdot 6H_2O$ (Tanaka Kikinzoku; 37.55% as Pt) and was irradiated with visible light for about 20 min in order to photodeposit the Ru, Rh, Ir, or Pt cocatalyst in situ. The apparent quantum yields (AQYs) defined by eq 1 were measured using filters combined with band-pass (Kenko) and cutoff (Hoya) filters and a photodiode (Ophira, PD300-UV head and Nova power monitor).

$$\text{AQY (\%)} = \frac{\text{number of reacted electrons}}{\text{number of incident photons}} \times 100 = \frac{\text{number of evolved } H_2 \text{ molecules} \times 2}{\text{number of incident photons}} \times 100 \quad (1)$$

3. Results and Discussion

3.1. $(CuAg)_xIn_{2x}Zn_{2(1-2x)}S_2$ Solid Solutions. Crystal Structures of $(CuAg)_xIn_{2x}Zn_{2(1-2x)}S_2$ Solid Solutions. $(CuAg)_xIn_{2x}Zn_{2(1-2x)}S_2$ solid solutions with an equimolar amount of Cu to Ag were synthesized. Figure 1 shows X-ray diffraction patterns for the ZnS and $(CuAg)_xIn_{2x}Zn_{2(1-2x)}S_2$ solid solutions ($x = 0.5-0.01$) synthesized at 1123 K. The

(13) Tsuji, I.; Kato, H.; Kobayashi, H.; Kudo, A. *J. Phys. Chem. B* **2005**, *109*, 7323.
(14) Reber, J. F.; Rusek, M. *J. Phys. Chem.* **1986**, *90*, 824.
(15) Kakuta, N.; Park, K. H.; Finlayson, M. F.; Ueno, A.; Bard, A. J.; Campion, A.; Fox, M. A.; Webber, S. E.; White, J. M. *J. Phys. Chem.* **1985**, *89*, 732.
(16) Maeda, K.; Takata, T.; Hara, M.; Saito, N.; Inoue, Y.; Kobayashi, H.; Domen, K. *J. Am. Chem. Soc.* **2005**, *127*, 8286.
(17) Maeda, K.; Teramura, K.; Takata, T.; Hara, M.; Saito, N.; Toda, K.; Inoue, Y.; Kobayashi, H.; Domen, K. *J. Phys. Chem. B* **2005**, *109*, 20504.
(18) Tsuji, I.; Kato, H.; Kudo, A. *Angew. Chem., Int. Ed.* **2005**, *44*, 3565.
(19) Xu, J. F.; Ji, W.; Lin, J. Y.; Tang, S. H.; Du, Y. W. *Appl. Phys. A* **1998**, *66*, 639.

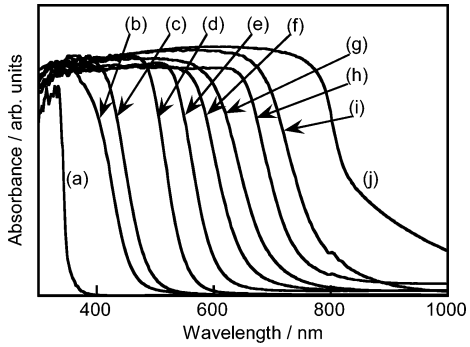

Figure 2. Diffuse reflectance spectra of $(CuAg)_xIn_{2x}Zn_{2(1-2x)}S_2$ solid solutions; the values of x were (a) 0, (b) 0.01, (c) 0.025, (d) 0.05, (e) 0.1, (f) 0.15, (g) 0.20, (h) 0.25, (i) 0.30, and (j) 0.5. The samples were synthesized in a quartz ampule tube at 1123 K.

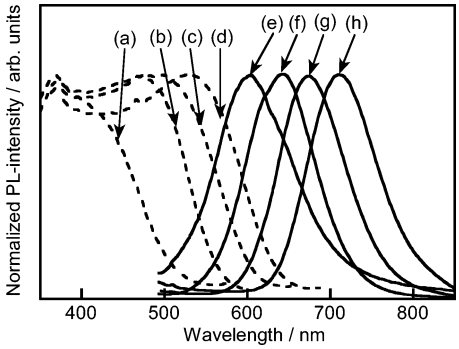

Figure 3. Photoluminescence spectra of $(CuAg)_xIn_{2x}Zn_{2(1-2x)}S_2$ solid solutions at 80 K. Excitation spectra were (a) $x = 0.025$ monitored at 600 nm, (b) $x = 0.05$ monitored at 640 nm, (c) $x = 0.10$ monitored at 675 nm, and (d) $x = 0.15$ monitored at 710 nm; emission spectra were (e) $x = 0.025$, (f) $x = 0.05$, (g) $x = 0.10$, and (h) $x = 0.15$, excited at 467 nm.

crystal structures of the solid solutions depended on the composition. The diffraction peaks of the solid solutions shifted to lower angles as the value of x was increased. The successive shift of the XRD pattern indicated that the crystals obtained were not mixtures of ZnS, $CuInS_2$, and $AgInS_2$ phases but the $(CuAg)_xIn_{2x}Zn_{2(1-2x)}S_2$ solid solutions. The solid solutions with small values of x such as $x = 0.01$ possessed a zinc-blende-type structure, as well as ZnS ($x = 0$). The wurtzite-type structure was obtained as the value of x was increased. When x was equal to or larger than 0.1, the solid solution became a single wurtzite-type phase. The solid solutions for $x = 0.025$ and 0.05 were mixtures of zinc blende and wurtzite. When the ratio of $CuInS_2$ and $AgInS_2$ to ZnS was increased, the symmetry of the crystal structure was no longer maintained, resulting in the formation of the wurtzite phase, which was confirmed around $x = 0.05$. The XRD pattern of $(CuAg)InS_2$ ($x = 0.5$) nearly corresponded to the chalcopyrite structures of $CuInS_2$ and $AgInS_2$.

Photophysical Properties of $(CuAg)_xIn_{2x}Zn_{2(1-2x)}S_2$ Solid Solutions. Figure 2 shows diffuse reflectance spectra of ZnS and $(CuAg)_xIn_{2x}Zn_{2(1-2x)}S_2$ solid solutions ($x = 0.01 \sim 0.5$). The solid solutions had intense absorption bands with steep edges in the visible light region, in contrast to ZnS, with its ultraviolet light absorption band. The steep shapes of the edges indicate that the visible light absorption was due to band gap transition not to the transition from impurity levels to the conduction band of ZnS, as observed for the metal-ion-doped ZnS photocatalysts.[8−10] The absorption edges of the solid solutions were shifted monotonically to longer wavelengths as the ratio of $MInS_2$ (M = Cu and Ag) to ZnS was increased. The band gaps of the solid solutions were estimated to be 2.68∼1.57 eV ($x = 0.01 \sim 0.3$) from the onsets of the absorption edges.

The $(CuAg)_xIn_{2x}Zn_{2(1-2x)}S_2$ solid solutions ($x = 0.025 \sim 0.1$) showed broad photoluminescence spectra at 80 K, as shown in Figure 3. The onset positions of the excitation spectra were almost the same as those of the diffuse reflectance spectra (Figure 2), indicating that the emission was derived from the band gap excitation. The excitation and emission spectra of the photoluminescence were shifted successively with the changing composition, as were those of the diffuse reflectance spectra. These properties of photoabsorption and photoluminescence suggest that the energy band structure of the $(CuAg)_xIn_{2x}Zn_{2(1-2x)}S_2$ solid solutions could be controlled by the composition as well as those of the previously reported $(MIn)_xZn_{2(1-x)}S_2$ (M = Cu or Ag) solid solutions.[12,13] We previously reported that the Cu 3d (Ag 4d) and In 5s5p orbitals contributed to the formation of the valence and conduction bands, respectively. Therefore, the $(CuAg)_xIn_{2x}Zn_{2(1-2x)}S_2$ solid solutions consisting of Cu and Ag should also have the same characteristic energy bands that contribute to a visible light response. The conduction band should consist of Zn 4s4p and In 5s5p, while the valence band should be composed of S 3p, Cu 3d, and Ag 4d. The proposed band structure of the $(CuAg)_xIn_{2x}Zn_{2(1-2x)}S_2$ solid solution was reasonable, judging from the fact that the diffuse reflectance and photoluminescence spectra were monotonically shifted to longer wavelengths as the ratio of $MInS_2$ (M = Cu and Ag) to ZnS was increased.

Table 1. Dependence of Photocatalytic Activities for H_2 Evolution from an Aqueous K_2SO_3 and Na_2S Solution over Pt (0.5 wt %)-loaded $(CuAg)_xIn_{2x}Zn_{2(1-2x)}S_2$ Solid Solutions upon the Value of x[a]

value of x	band gap (eV)	rate of H_2 evolution/ μmol h^{-1}
0	3.50	1.6
0.01	2.68	152
0.025	2.54	134
0.05	2.24	130
0.1	2.05	135
0.15	1.90	119
0.20	1.77	71
0.25	1.66	43
0.30	1.57	22
0.5	1.43	0

[a] Catalysts: 0.3 g, synthesized in quartz ampule tube at 1123 K; reactant solution, 150 mL (0.5 mol L^{-1} K_2SO_3 + 0.1 mol L^{-1} Na_2S); light source, 300-W Xe lamp with a cutoff filter ($\lambda \geq 420$ nm).

Photocatalytic Activities of $(CuAg)_xIn_{2x}Zn_{2(1-2x)}S_2$ Solid Solutions. Table 1 shows the effect of composition on the photocatalytic activities of Pt cocatalyst (0.5 wt %)-loaded $(CuAg)_xIn_{2x}Zn_{2(1-2x)}S_2$ solid solutions for H_2 evolution from an aqueous solution containing SO_3^{2-} and S^{2-} ions as sacrificial reagents. The solid solutions showed relatively high activities for H_2 evolution under visible light irradiation ($\lambda \geq 420$ nm), although ZnS ($x = 0$) and $(CuAg)_{0.5}InS_2$ ($x = 0.5$) showed little activity. The photocatalytic activities of the solid solutions depended on the composition as well as the photophysical properties. The photocatalytic activity increased gradually when the compositional parameter x was decreased from 0.5 to 0.1. The change in the activity for H_2

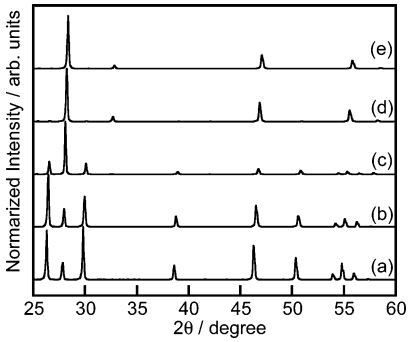

Figure 4. X-ray diffraction patterns of $Cu_xAg_yIn_{0.4}Zn_{2(1-x-y)}S_2$ solid solutions; the values of x and y were (a) 0 and 0.4, (b) 0.1 and 0.3, (c) 0.2 and 0.2, (d) 0.3 and 0.1, and (e) 0.4 and 0. The samples were synthesized in a quartz ampule tube at 1123 K.

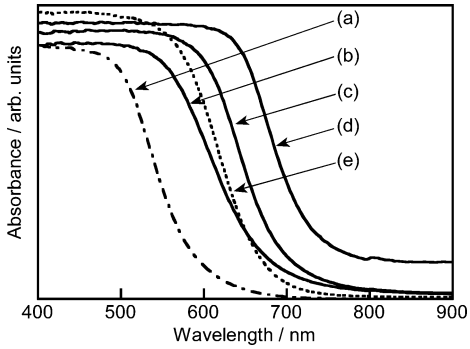

Figure 5. Diffuse reflectance spectra of $Cu_xAg_yIn_{0.4}Zn_{2(1-x-y)}S_2$ solid solutions; the values of x and y were (a) 0 and 0.4, (b) 0.1 and 0.3, (c) 0.2 and 0.2, (d) 0.3 and 0.1, and (e) 0.4 and 0. The samples were synthesized in a quartz ampule tube at 1123 K.

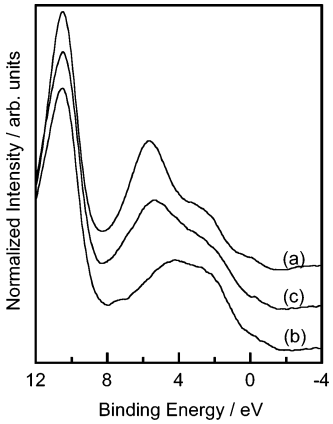

Figure 6. X-ray photoelectron spectra of $Cu_xAg_yIn_{0.4}Zn_{2(1-x-y)}S_2$ solid solutions; the values of x and y were (a) 0 and 0.4, (b) 0.4 and 0, and (c) 0.2 and 0.2. The samples were synthesized in a quartz ampule tube at 1123 K.

evolution was due to the conduction band level of the solid solutions. In other words, the photocatalytic activity increased with the formation of the conduction band, which was high enough to reduce H_2O to form H_2 as the ratio of ZnS was increased. The activities of the solid solution photocatalysts ($x = 0.01 \sim 0.1$) were almost the same as each other, because they might be affected not only by the conduction band level but also other factors. One negative factor for the photocatalytic performance is that the number of available photons decreases with the widening of the band gap. Another negative factor is that the energy bands consisting of Cu, Ag, and In became discontinuous as the value of x became small. This would result in a decrease in the mobility of the photogenerated carriers, which is an important factor affecting the photocatalytic activity. The crystal structure, zinc blende and wurtzite, which depended upon the composition, would also affect the charge separation and migration of photogenerated carriers.

3.2. $Cu_xAg_yIn_{0.4}Zn_{1.2}S_2$ Solid Solutions. Crystal Structures of $Cu_xAg_yIn_{0.4}Zn_{1.2}S_2$ Solid Solutions. $Cu_xAg_yIn_{0.4}Zn_{1.2}S_2$ solid solutions for which the composition $x + y$ was fixed at 0.4 were synthesized. Figure 4 shows the X-ray diffraction patterns of the $Cu_xAg_yIn_{0.4}Zn_{1.2}S_2$ solid solutions synthesized at 1123 K. The solid solution $Ag_{0.4}In_{0.4}Zn_{1.2}S_2$, containing only Ag as a monovalent element, had a single-phase wurtzite structure. On the other hand, the solid solution $Cu_{0.4}In_{0.4}Zn_{1.2}S_2$, containing only Cu as the monovalent element, had a single-phase zinc blende structure. The crystal structures of $Cu_{0.1}Ag_{0.3}In_{0.4}Zn_{1.2}S_2$, $Cu_{0.2}Ag_{0.2}In_{0.4}Zn_{1.2}S_2$, and $Cu_{0.3}Ag_{0.1}In_{0.4}Zn_{1.2}S_2$ solid solutions depended on the ratio of Cu to Ag. The diffraction peaks were shifted to higher angles as the ratio of Cu was increased, indicating that the crystals obtained were not mixtures of ZnS, $CuInS_2$, and $AgInS_2$ phases but were the $Cu_xAg_yIn_{0.4}Zn_{1.2}S_2$ solid solutions. The shift was reasonable, because the ionic radius of Cu^+ (0.74 Å) is smaller than that of Ag^+ (1.14 Å).[20]

Photophysical Properties of $Cu_xAg_yIn_{0.4}Zn_{1.2}S_2$ Solid Solutions. Figure 5 shows diffuse reflectance spectra for the $Cu_xAg_yIn_{0.4}Zn_{1.2}S_2$ solid solutions. $Cu_{0.4}In_{0.4}Zn_{1.2}S_2$ has an absorption band at a longer wavelength than $Ag_{0.4}In_{0.4}Zn_{1.2}S_2$, because the valence band composed of the Cu 3d and S 3p hybrid orbitals was formed at a more negative level than that of Ag 4d and S 3p hybrid orbitals. Therefore, it would be expected that the absorption edges of $Cu_xAg_yIn_{0.4}Zn_{1.2}S_2$ solid solutions, consisting of both Cu and Ag, would have shifted to longer wavelengths as the ratio of Cu to Ag had been increased. However, contrary to the expectation, the absorption edges for $Cu_xAg_yIn_{0.4}Zn_{1.2}S_2$ were at longer wavelengths than that of $Cu_{0.4}In_{0.4}Zn_{1.2}S_2$. The unexpected red shift should be due to a widening of the valence band by the interaction between the Cu 3d and Ag 4d orbitals. Another possible reason is that the crystal fields around the monovalent Cu^+ and Ag^+ ions changed when these ions existed in the solid solutions consisting of Cu and Ag. The energetically stable crystal phase of the solid solution containing either Cu or Ag is zinc blende or wurtzite. On the contrary, in the solid solutions containing both Cu and Ag, these monovalent ions must exist in a crystal phase that is unstable, and thus, the crystal fields around the monovalent ions could be different from those in the stable crystal phase. The changes in the crystal fields should affect the energy states of the Cu 3d and Ag 4d orbitals, which contribute to the valence band formation.

The X-ray photoelectron spectra of $Cu_xAg_yIn_{0.4}Zn_{2(1-x-y)}S_2$ solid solutions were measured in order to examine their valence band states (Figure 6). The solid solution of $Ag_{0.4}In_{0.4}Zn_{1.2}S_2$ has a distinctive peak at around 5.7 eV, which is assigned to Ag 4d, and a small shoulder on the lower-energy side. The solid solution of $Cu_{0.4}In_{0.4}Zn_{1.2}S_2$ showed

(20) Shannon, R. *Acta Crystallogr., Sect. A* **1976**, *32*, 751.

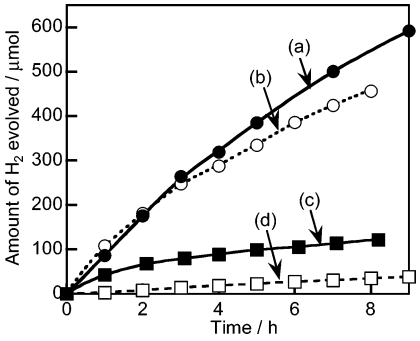

Figure 7. Photocatalytic H_2 evolution under visible light irradiation over the (a) Pt (0.5 wt %)/$(CuAg)_{0.15}In_{0.3}Zn_{1.4}S_2$, (b) Pt (0.5 wt %)/$Cu_{0.1}Ag_{0.3}In_{0.4}Zn_{1.2}S_2$, (c) Pt (0.5 wt %)/$(AgIn)_{0.6}Zn_{0.8}S_2$, and (d) Pt (0.5 wt %)/$(CuIn)_{0.4}Zn_{1.2}S_2$ photocatalysts. Reactant solution, $K_2SO_3-Na_2S$ (0.5 mol L^{-1}/0.1 mol L^{-1}) aqueous solution (150 mL); catalyst, 0.3 g; light source, 300-W Xe lamp with a cutoff filter ($\lambda \geq 420$ nm); reaction cell, Pyrex cell with a top window.

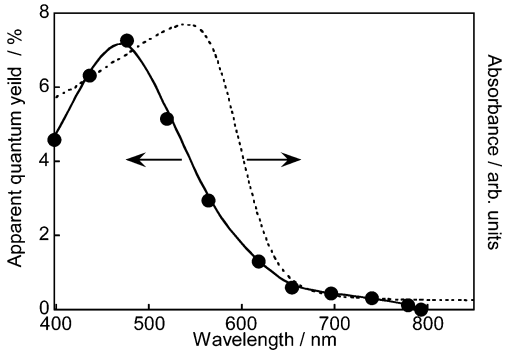

Figure 8. Action spectrum of H_2 evolution from an aqueous $K_2SO_3-Na_2S$ (0.25 mol L^{-1}/0.35 mol L^{-1}) solution (150 mL) over the Pt (5 wt %)−$(CuAg)_{0.15}In_{0.3}Zn_{1.4}S_2$ photocatalyst; catalyst, 0.3 g; light source, 300-W Xe lamp with cutoff and band-pass filters; reaction cell, Pyrex cell with a top window.

a broad peak at lower energy compared to that of $Ag_{0.4}In_{0.4}Zn_{1.2}S_2$, because the Cu 3d orbitals tend to contribute near the valence band maximum (highest occupied molecular orbital). Our previous studies for ZnS−$AgInS_2$ and ZnS−$CuInS_2$ solid solutions revealed that Ag 4d + S 3p and Cu 3d + S 3p hybrid orbitals make up of the valence bands. The photoelectron spectrum of $Cu_{0.2}Ag_{0.2}In_{0.4}Zn_{1.2}S_2$, combining Cu and Ag, has a peak assigned to Ag 4d, as in $Ag_{0.4}In_{0.4}Zn_{1.2}S_2$, and a comparatively broad shoulder on the low-energy side, similar to that of $Cu_{0.4}In_{0.4}Zn_{1.2}S_2$. This result suggests that the valence band of the $Cu_{0.2}Ag_{0.2}In_{0.4}Zn_{1.2}S_2$ solid solution is composed of both Cu 3d and Ag 4d orbitals. The spectrum of $Cu_{0.2}Ag_{0.2}In_{0.4}Zn_{1.2}S_2$ in the valence region is wider than those of $Cu_{0.4}In_{0.4}Zn_{1.2}S_2$ and $Ag_{0.4}In_{0.4}Zn_{1.2}S_2$. Inoue et al. reported that the $ZnGa_2O_4$ photocatalyst has a narrower band gap than $SrGa_2O_4$, because of the interaction of energy bands composing the valence band.[21] Therefore, the Zn 3d energy band may also widen the valence band in addition to the interaction between Cu 3d and Ag 4d energy bands, resulting in raising the valence band maximum and the red shift of the absorption band, as shown in Figure 5.

Photocatalytic Activities of $Cu_xAg_yIn_{x+y}Zn_{2(1-x-y)}S_2$ Solid Solutions. The red shift of the absorption band that results from the combination of Cu and Ag in the series of solid solutions is a useful property for the utilization of the solar spectrum. Figure 7 shows the photocatalytic hydrogen evolution results for the solid solutions with similar narrow band gaps (1.8−1.9 eV). Pt/$Ag_{0.6}In_{0.6}Zn_{0.8}S_2$ (BG: 1.84 eV) and Pt/$Cu_{0.4}In_{0.4}Zn_{1.2}S_2$ (BG: 1.84 eV) showed low activities for H_2 evolution. In contrast, Pt/$Cu_{0.15}Ag_{0.15}In_{0.3}Zn_{1.4}S_2$ (BG: 1.90 eV) and Pt/$Cu_{0.1}Ag_{0.3}In_{0.4}Zn_{1.2}S_2$ (BG: 1.82 eV) showed relatively high activities, even though their band gaps were as narrow as those of $Ag_{0.6}In_{0.6}Zn_{0.8}S_2$ and $Cu_{0.4}In_{0.4}Zn_{1.2}S_2$. The differences in the activities among these solid solutions can be ascribed to the band structures. The conduction band level depends on the ratio of In to Zn whose orbitals, Zn 4s4p and In 5s5p, contribute to the conduction band formation. The photocatalytic activity tended to increase with the formation of the conduction band of which the energy level was high enough to reduce H_2O to form H_2 as the ratio of ZnS increased, as seen in Table 1. Therefore, the $Cu_{0.15}Ag_{0.15}In_{0.3}Zn_{1.4}S_2$ solid solution, which has a comparatively high conduction band level because of the large ratio of Zn, could show a high photocatalytic activity. On the other hand, the crystal structure is also another possible factor affecting the band gap. In some sulfides, such as ZnS, CdS, and $AgInS_2$, which have a crystal structure similar to that of the present solid solution, the band gaps of the high-temperature phase (wurtzite-type) are ca. 0.1 eV wider than that of the low-temperature phase (zinc blende or chalcopyrite-type).[22,23] Therefore, it can be expected that the conduction band level of wurtzite-type $Cu_{0.1}Ag_{0.3}In_{0.4}Zn_{1.2}S_2$ might be higher than that of zinc-blende-type $Cu_{0.4}In_{0.4}Zn_{1.2}S_2$, even though the In/Zn ratios are the same, with the result that the $Cu_{0.1}Ag_{0.3}In_{0.4}Zn_{1.2}S_2$ solid solution shows high photocatalytic activity. The valence bands of the $Cu_{0.15}Ag_{0.15}In_{0.3}Zn_{1.4}S_2$ and $Cu_{0.1}Ag_{0.3}In_{0.4}Zn_{1.2}S_2$ solid solutions should be located at higher energies than those of $Cu_{0.4}In_{0.4}Zn_{1.2}S_2$ and $Ag_{0.6}In_{0.6}Zn_{0.8}S_2$, due either to the interaction between the Cu 3d and Ag 4d orbitals or changes in the crystal fields around these metals, as discussed above. The increase in the mobility of photogenerated holes that would result from the extension of the valence band will also be a positive factor.

Figure 8 shows an action spectrum for H_2 evolution from an aqueous solution containing both K_2SO_3 and Na_2S over the Pt (5 wt %)-loaded $Cu_{0.15}Ag_{0.15}In_{0.3}Zn_{1.4}S_2$ solid solution photocatalyst, together with its diffuse reflectance spectrum. The latter was measured for a sample mixed with barium sulfate, because the absorption otherwise saturated. The action spectrum clearly rose at the edge of the absorption band, indicating that the visible light response for hydrogen evolution is attributable to the band gap transition between the valence and conduction bands, which is controllable with a change in the composition. H_2 evolved even through the absorption tail in the region around 650−750 nm. This response was probably due to transitions between the energy bands of the solid solution and defect or impurity levels.

3.3. Optimization of Photocatalytic Activity. To optimize the photocatalytic activity, the effect of metal cocatalysts

(21) Ikarashi, K.; Sato, J.; Kobayashi, H.; Saito, N.; Nishiyama, H.; Inoue, Y. *J. Phys. Chem. B* **2002**, *106*, 9048.

(22) Shionoya, S.; Yen, W. M. *Phosphor Handbook*; CRC: New York, 1999.

(23) Shay, J. L.; Tell, B.; Schiavone, L. M. *Phys. Rev. B* **1974**, *9*, 1719.

Table 2. Effects of Reaction and Preparation Conditions on Photocatalytic Activities of $(CuAg)_{0.15}In_{0.3}Zn_{1.4}S_2$ Solid Solution[a]

preparation condition	BET/ m^{-2} g^1	cocatalyst		rate of H_2 evolution/ μmol h^{-1}
1123 K/5 h	0.2	none		30
1123 K/5 h	0.2	Ru	(0.5 wt %)	660
1123 K/5 h	0.2	Rh	(0.5 wt %)	720
1123 K/5 h	0.2	Ir	(0.5 wt %)	40
1123 K/5 h	0.2	Pt	(1.0 wt %)	340
1123 K/5 h	0.2	Ru	(0.5 wt %)	660
923 K/5 h	2.0	Ru	(0.5 wt %)	1160
873 K/5 h	3.8	Ru	(0.5 wt %)	1420
773 K/5 h	5.7	Ru	(0.5 wt %)	2320
673 K/5 h	7.9	Ru	(0.5 wt %)	1080

[a] Catalyst, 0.3 g; reactant solutions, 150 mL (0.25 mol L^{-1} K_2SO_3 + 0.35 mol L^{-1} Na_2S); light source, 300-W Xe lamp with a cutoff filter ($\lambda \geq$ 420 nm).

other than Pt and the effect of the synthesis temperature were investigated, as shown in Table 2. Ru, Rh, and Ir were photodeposited as cocatalysts. The $(CuAg)_{0.15}In_{0.3}Zn_{1.4}S_2$ solid solution showed photocatalytic activity for H_2 evolution even without a cocatalyst (30 μmol h^{-1}). The photocatalytic activity was much improved by Ru and Rh loading, just as with Pt loading. The Rh-loaded photocatalyst showed the highest activity, although a deactivation was observed during the photocatalytic reaction. The Ru-loaded photocatalyst showed higher photocatalytic activity than the Pt-loaded photocatalyst, and comparatively steady activity was obtained. On the contrary, the Ir loading was not effective for the photocatalytic reaction. Iridium does not possess an excellent ability to act as a catalytically active site for H_2 evolution because the hydrogen overvoltage is largest among the metals employed as cocatalysts.[24] It has also been reported that the effect of the deposition of Ir on the photocatalytic H_2 evolution activity of TiO_2 from an aqueous solution containing 2-propanol was smaller than those of Pt, Ru, and Rh metal cocatalysts.[25]

The photocatalyst was synthesized at various temperatures in order to improve the photocatalytic activity. A lower synthesis temperature improved the photocatalytic activity, as shown in Table 2. The maximum activity was obtained at 773 K. The initial rate of H_2 evolution was more than 2 mmol h^{-1}. The surface areas were increased by lowering of the synthesis temperature, as seen in Table 2, suggesting that the particle size became small. Figure 9 shows X-ray diffraction patterns of $(CuAg)_{0.15}In_{0.3}Zn_{1.4}S_2$ solid solutions synthesized at different temperature. The solid solution synthesized at 773 K possessed a certain degree of good crystallinity judging from the diffraction peaks. However, the solid solution had a small amount of liberated $AgInS_2$, indicating the incompletion of solid solution formation. The formation of the $AgInS_2$ impurity was more noticeable in the synthesis carried out at 673 K. The $AgInS_2$ impurity shielded incident light and acted as a recombination site for photogenerated carriers, resulting in a drastic decrease in the photocatalytic activity. Figure 10 shows SEM images of the $(CuAg)_{0.15}In_{0.3}Zn_{1.4}S_2$ solid solution synthesized at 1123 and

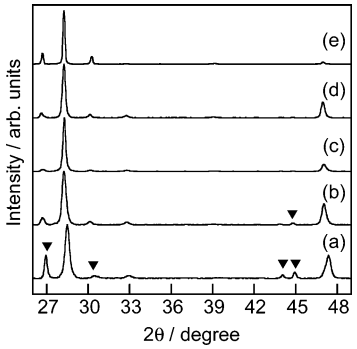

Figure 9. X-ray diffraction patterns of $(CuAg)_{0.15}In_{0.3}Zn_{1.4}S_2$ solid solutions synthesized at (a) 673 K, (b) 773 K, (c) 873 K, (d) 923 K, and (e) 1123 K in a quartz ampule tube. Triangles indicate $AgInS_2$.

773 K. The solid solution synthesized at 1123 K possessed well-crystallized large particles in the size range of ca. 10−30 μm, as shown in Figure 10a. On the other hand, nanoparticles were obtained by the low-temperature synthesis at 773 K, as shown in Figure 10b. Most small particles had sharp edges and clear planes, showing that they were well-crystallized. Even though the low-temperature synthesis was carried out, a certain degree of crystallinity was confirmed by the SEM image and the intensity of the X-ray diffraction. Therefore, the small, well-crystallized particles contributed to the high photocatalytic activity. The photocatalytic activities of previously reported $(MIn)_xZn_{2(1-x)}S_2$ (M = Cu or Ag) solid solutions consisting of Ag or Cu were never improved by synthesis temperatures lower than 873 K. Therefore, the improvement of photocatalytic activity by the low-temperature synthesis is a characteristic behavior of the $CuInS_2$−$AgInS_2$−ZnS solid solution system.

When the efficient use of visible light is taken into account, the $(CuAg)_{0.25}In_{0.5}ZnS_2$ solid solution, which had an absorption band at a wavelength longer than that of the $(CuAg)_{0.15}In_{0.3}Zn_{1.4}S_2$ solid solution, was synthesized. The $(CuAg)_{0.25}In_{0.5}ZnS_2$ solid solution synthesized at 873 K was a mixture of zinc blende and wurtzite structures. A small amount of $AgInS_2$ impurity was observed. The BET surface area was 1.6 m^2 g^{-1}. The absorption edge of the solid solution was observed at ca. 700 nm (band gap, 1.77 eV). Figure 11 shows the dependence of the rate of H_2 evolution upon the amount of Ru cocatalyst loaded on the $Cu_{0.25}Ag_{0.25}In_{0.5}ZnS_2$ photocatalyst and the time course of H_2 evolution on the Ru (1 wt %)-loaded photocatalyst. The photocatalytic activity of the nonloaded photocatalyst was low (11 μmol h^{-1}). On the contrary, the photocatalytic activity was much improved by increasing the amount of Ru below 1 wt %. The photocatalytic activity of the Ru (1.5 wt %)-loaded photocatalyst was quite high at the initial stage (2.8 mmol h^{-1}), but a comparatively large deactivation was observed during the reaction, probably because of a shielding effect of the Ru cocatalyst. On the other hand, the Ru (1 wt %)-loaded photocatalyst showed high activity with only a slight deactivation. Even under simulated solar irradiation (AM 1.5), the solid solution photocatalyst showed high activity for H_2 evolution: the initial rate of H_2 evolution was 7.9 L m^{-2} h^{-1}.

The electrolysis of an aqueous K_2SO_3−Na_2S (0.25 mol L^{-1}/0.35 mol L^{-1}) solution (100 mL) with a polycrystalline

(24) Bockris, J. O.; Drazic, D. M. *Electro-Chemical Science*; Taylor and Francis: London, 1972.
(25) Teratani, S.; Nakamichi, J.; Taya, K.; Tanaka, K. *Bull. Chem. Soc. Jpn.* **1982**, *55*, 1688.

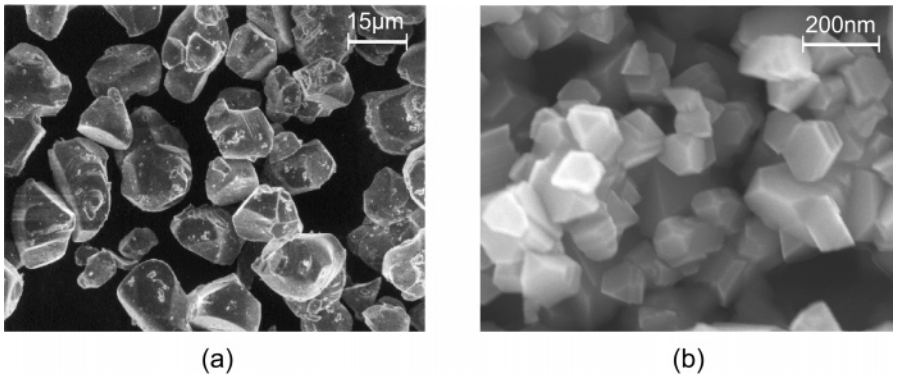

Figure 10. Scanning electron microscope images of the $(CuAg)_{0.15}In_{0.3}Zn_{1.4}S_2$ solid solution synthesized in a quartz ampule tube at (a) 1123 K and (b) 773 K.

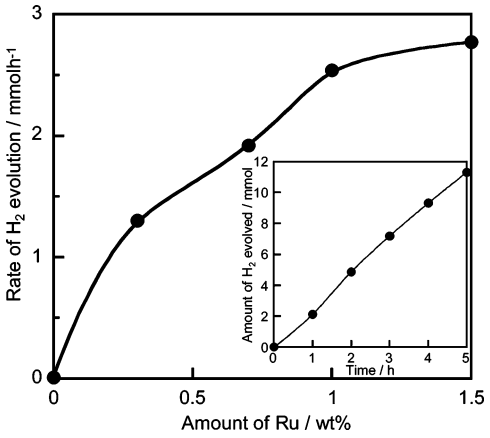

Figure 11. Dependence of the rate of H_2 evolution upon the amount of Ru cocatalyst loaded on the $Cu_{0.25}Ag_{0.25}In_{0.5}ZnS_2$ solid solution and (inset) the time course of H_2 evolution over the Ru (1 wt %)-loaded $Cu_{0.25}Ag_{0.25}In_{0.5}ZnS_2$ photocatalyst; reactant solution, $K_2SO_3-Na_2S$ (0.5 mol L^{-1}/0.1 mol L^{-1}) aqueous solution (150 mL); catalyst, 0.3 g; light source, 300-W Xe lamp with a cutoff filter ($\lambda \geq 420$ nm); reaction cell, Pyrex cell with a top window.

silicon solar cell (Toei, 47 cm^2; V_{oc}, 1.7 V; I_{sc}, 450 mA) and Pt electrodes (1×1 cm^2) was investigated under simulated solar irradiation (AM 1.5) to compare H_2 production on the solid solution photocatalyst with that by electrolysis. H_2 gas evolved from the cathode electrode; the initial current was 5 mA. However, the current gradually decreased to 1 mA after 60 min. This was due to the blocking of the anode by sulfur deposition (anode passivation). The rate of H_2 evolution during electrolysis with the solar cell was ca. 0.1 L m^{-2} h^{-1}, which was calculated from the steady-state current (1 mA) after 60 min. This rate was considerably lower than the photocatalytic H_2 evolution obtained for the solid solution photocatalyst (7.9 L m^{-2} h^{-1}).

Conclusions

The authors have previously reported that the series of $ZnS-MInS_2$ (M = Cu or Ag) solid solutions were active photocatalysts for H_2 evolution under visible light irradiation. In the present study, $ZnS-CuInS_2-AgInS_2$ solid solutions that were able to respond to a wide range of visible light wavelengths were developed. The crystal structure and the energy band structure of the solid solution depended upon the composition. The narrower band gap of the $ZnS-CuInS_2-AgInS_2$ solid solution compared with those of $ZnS-MInS_2$ (M = Cu or Ag) solid solutions was probably due to the interaction between Cu 3d and Ag 4d orbitals in the valence band. The photocatalytic activity of the $ZnS-CuInS_2-AgInS_2$ solid solution was higher than those of the previously reported $ZnS-MInS_2$ (M = Cu or Ag) solid solutions. The Ru-loaded $Cu_{0.25}Ag_{0.25}In_{0.5}ZnS_2$ photocatalyst, with the narrow band gap of 1.77 eV, efficiently produced H_2 gas (7.9 L m^{-2} h^{-1}) even under simulated solar irradiation.

Acknowledgment. This work was supported by the Core Research for Evolutional Science and Technology (CREST) program of the Japan Science and Technology Agency (JST) and a Grant-in-Aid for Priority Area Research (No. 417) from the Ministry of Education, Culture, Science, and Technology of Japan.

CM0527017